



ELSEVIER

Available online at www.sciencedirect.com

Proceedings of the Combustion Institute xxx (2010) xxx–xxx

**Proceedings
of the
Combustion
Institute**

www.elsevier.com/locate/proci

Chemistry and kinetics of chemical vapor deposition of pyrolytic carbon from ethanol

A. Li^a, S. Zhang^c, B. Reznik^a, S. Lichtenberg^a, G. Schoch^a,
O. Deutschmann^{a,b,*}

^a Institute for Chemical Technology and Polymer Chemistry (ITCP), Karlsruhe Institute of Technology (KIT),
PF 6980, 76049 Karlsruhe, Germany

^b Institute for Nuclear and Energy Technologies (IKET), Karlsruhe Institute of Technology (KIT), PF 6980,
76049 Karlsruhe, Germany

^c Northwestern Polytechnical University (NPU), Youyixi 127, 710072, Xi'an, China

Abstract

Synthesis of pyrolytic carbon as a matrix for carbon fiber reinforced carbon composites by chemical vapor infiltration (CVI) is experimentally and numerically studied using the oxygen-containing precursor ethanol. The effects of residence time on microstructure and deposition rate of pyrolytic carbon are investigated. A short residence time is found to favor the formation of high-textured pyrolytic carbon. The evolutions of microstructure and deposition rate of pyrolytic carbon are compared with those of carbon deposited from methane. Compared to methane, ethanol exhibits a much higher deposition rate of pyrolytic carbon with similar microstructures. Pyrolysis of ethanol is modeled using a two-dimensional flow model coupled with a detailed gas-phase reaction mechanism involving 261 species taking part in 1177 reversible reactions. Reaction rate analysis reveals that C₃ hydrocarbons are the most important intermediate species contributing to the maturation of gas-phase composition. A comparison of the kinetic predictions with equilibrium calculations demonstrates that the pyrolysis of ethanol in the synthesis reactor applied is far away from equilibrium.

© 2010 The Combustion Institute. Published by Elsevier Inc. All rights reserved.

Keywords: Carbon composite; Kinetics; Pyrolysis; Reaction rate analysis

1. Introduction

Kinetics of ethanol combustion has been extensively studied numerically in the literature. Marinov [1] presented a detailed reaction mechanism

emphasizing that high temperature ethanol oxidation is strongly sensitive to the falloff kinetics of the ethanol decomposition process and to the branching ratio assignments among the ethanol abstraction reactions. Recent work by Li et al. [2] showed that H₂O and C₂H₄ are the major products of ethanol thermal decomposition at temperatures ranging from 1045 to 1080 K, and it was reported that the molecular decomposition reaction C₂H₅OH → C₂H₄ + H₂O strongly depends on temperature and is the dominant reaction pathway at temperatures ranging from 300 to 2500 K at

* Corresponding author at: Institute for Chemical Technology and Polymer Chemistry (ITCP), Karlsruhe Institute of Technology (KIT), PF 6980, 76049 Karlsruhe, Germany. Fax: +49 721 6084805.

E-mail address: Deutschmann@kit.edu (O. Deutschmann).

1 atm. Based on comparison of conversion and deposit formation of ethanol and butane, Gupta et al. found that there is no significant production of species containing more than two carbon atoms during the pyrolysis of ethanol, whereas propylene production is significant during the pyrolysis of butane at temperatures ranging from 973 to 1073 K [3]. Other previous work, however, reveals that the use of ethanol as an oxygenate additive to diesel fuel appears to be less desirable, since ethanol may contribute to particulate carbon formation [4] and easily form soot at elevated pressures making ethanol an ideal candidate precursor for the formation of pyrolytic carbon.

Chemical vapor deposition is the most common process for the synthesis of carbon/carbon composites, in which hydrocarbons are usually employed as carbon precursors [5–7]. At high temperatures, two general mechanisms for carbon deposition exist [7]. Firstly, carbon can be formed as a result of light hydrocarbon species reacting at substrate edges on active sites. This process has been very well studied with low pressure CVD experiments using methane, ethylene, acetylene, propane, and 1,3-butadiene [8–10], and more recently the results were taken as a basis for modeling the CVD/CVI process of pyrolytic carbon [11–13]. The CVD mechanism of each hydrocarbon involves pyrolysis of the initial carbon precursor, maturation of the gas-phase composition, chemical adsorption of possible light carbon sources onto active sites of surface edges, and finally the formation of carbon by dehydrogenation of surface species. Secondly, gas-phase reactions may lead to formation of species with higher molecular weight, e.g., aromatics and polycyclic aromatic hydrocarbons (PAH), which may act as carbon precursors [7]. These reactions are most important for the deposition of carbon from hydrocarbons at higher partial pressures because of the premature gas-phase composition. This process is usually initiated by gas-phase nucleation at high temperatures followed by physical adsorption of these nuclei on the substrate surface. Therefore, no matter which mechanism is proposed, the evolution of the gas-phase composition determines the precursors of the carbon deposits. In this context, it is essential to characterize the gas-phase chemistry and kinetics of the pyrolysis of ethanol and to understand how such reactions can influence the formation of pyrolytic carbon from ethanol.

In the present work, CVD experiments were performed to study the effect of residence time on the microstructure and the deposition rate of pyrolytic carbon from ethanol. In ethanol, the presence of the hydroxyl group leads to weaker C–H bonds, suggesting it might be much more reactive than C₂ hydrocarbons [3]. One might also expect that the presence of oxygen in ethanol will more or less suppress carbon deposition. A reaction rate analysis using detailed gas-phase chemi-

cal kinetics to identify the key steps and species leading to molecular weight growth in ethanol pyrolysis is performed. Experimental investigation of pyrolytic carbon deposition from ethanol as well as modeling the pyrolysis of ethanol offer opportunities to study the fundamental behavior of an oxygen-containing carbon precursor and the influence of an oxygen-containing additive on the deposition of pyrolytic carbon from light hydrocarbons.

2. Experimental setup and characterization methods

2.1. Setup and materials

The pyrolysis/deposition experiments were performed using a vertical flow reactor consisting of a ceramic tube with an inner diameter of 8.6 mm, heated by a furnace with a length of 30 cm. Bundles of high modulus carbon fibers (Toray M40-3k) were used as the substrate/precursor. Ethanol was vaporized into a stream of argon. The wall temperature profile of the inner tube was measured using a k-type thermocouple. Figure 1(a) shows the scheme of the CVD reactor and Fig. 1(b) shows the wall temperature profiles of the reactor measured for two residence times. One can recognize that shortening the residence time by a factor of 4 has only little influence on the temperature profile of the reactor. This experimental study mainly focuses on the influence of the residence time (0.025–0.125 s), therefore the ethanol partial pressure of 5 kPa and the total pressure of 10 kPa were kept constant. The residence time is determined by

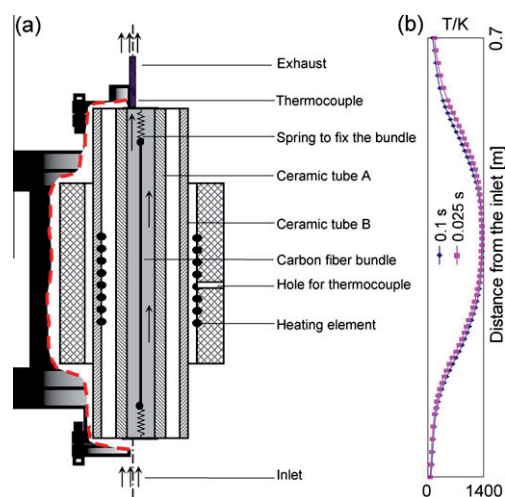


Fig. 1. Scheme of the experimental setup for densification of carbon fiber bundles (a) and the axial temperature profiles of the reactor resulting from two different residence times (b).

$$139 \quad \tau = V_R / \dot{V}_f \quad (1)$$

140 where τ is the residence time, V_R the volume of the
 141 isothermal part of the reactor chamber (approximately 5 cm in length), and \dot{V}_f the volumetric flow
 142 rate of the feed at reaction conditions. After 10 h
 143 of densification, carbon fiber bundles were taken
 144 out of the reactor, and the densified parts of the
 145 bundles were then cut along the axial direction
 146 into several small pieces to determine textures
 147 and the mean deposition rate of carbon as function
 148 of the position in the reactor. In comparison,
 149 two additional experiments using methane as pre-
 150 cursor were also performed at a residence time of
 151 0.125 s, a total pressure of 5 and 10 kPa, and a
 152 deposition time of 30 h.
 153

154 2.2. Determination of texture and deposition rate

155 Pyrolytic carbon deposits exhibit a broad variety
 156 of microstructures. A clear characterization of
 157 the microstructures is a precondition to establish a
 158 correlation between the microstructure formed
 159 and the deposition conditions. The microstructure
 160 of pyrolytic carbon deposits can be analyzed by
 161 polarized light microscopy (PLM) on polished
 162 cross-sections of the derived samples. The
 163 extracted increasing extinction angle A_e correlates
 164 with the increasing texture degree of pyrolytic
 165 carbon deposits, and three common types of laminar
 166 pyrolytic carbon deposits can be distinguished as
 167 shown in Fig. 2(a): low, medium, and high-textured
 168 (LT, MT, and HT) according to the present
 169 terminology and dark laminar (DL), smooth laminar
 170 (SL), and rough laminar (RL) according to the
 171 former terminology, respectively [7,14]. The
 172 orientation of graphitic stacks in high-textured
 173 carbon is much more preferable to their orientation
 174 in low-textured carbon. For a quantitative
 175 characterization of the carbon matrix in the present
 176 work, the extinction angle A_e at cross-sections
 177 of each sample was determined by polarized light
 178 microscopy (PLM) using an improved measure-
 179 ment technique [15] using digital monitoring of
 180 light extinctions as it shown in Fig. 2(b). A
 181 description of the method can be found elsewhere
 182 [14,15]. In case of a completely circular fiber cross-
 183 section, the systematic measurement error is about
 184 $\pm 1^\circ$. Since fibers are not circular in reality,
 185 the actual error is in the range of $\pm 1.5^\circ$. The mean
 186 deposition rate of the carbon matrix was also
 187 determined from PLM and the systematic error
 188 is in the range of $\pm 1 \mu\text{m}$.

189 3. Experimental results

190 3.1. Microstructure of pyrolytic carbon

191 The residence time has a significant impact on
 192 the evolution of the gas-phase composition during

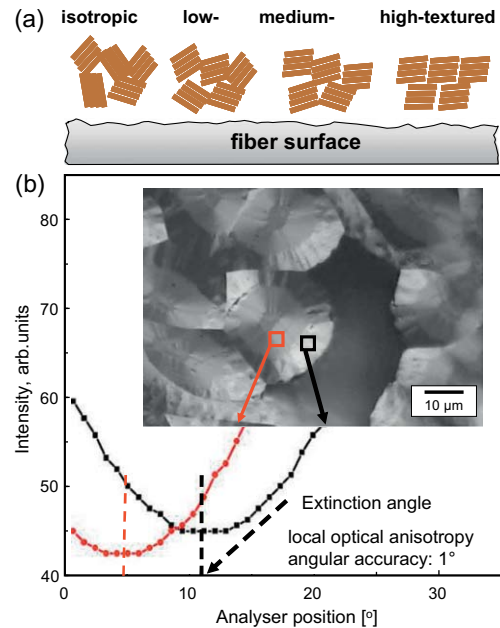


Fig. 2. Schematic presentation of preferred orientations of the graphitic stacks in pyrolytic carbon deposits (a) and digital determination of the extinction angle (A_e) using the improved PLM technique [15] (b).

193 high temperature pyrolysis of light linear hydro-
 194 carbons such as ethylene [10,11]. The hydroxyl
 195 group in ethanol weakens C-H bonds, suggesting
 196 that the pyrolysis of ethanol may be more sensi-
 197 tive to the residence time at high temperatures
 198 than in case of hydrocarbons. As a consequence,
 199 the residence time is expected to also have a major
 200 impact on carbon deposition from ethanol. Sev-
 201 eral experiments were performed with a deposi-
 202 tion time of 10 h and an ethanol partial pressure
 203 of 5 kPa at a total pressure of 10 kPa. Figure 3
 204 presents the evolution of the extinction angle of
 205 pyrolytic carbon along the axis of the fiber bundle
 206 synthesized using various residence times. It is
 207 obvious that a short residence time generally
 208 favors the formation of HT carbon. One distin-
 209 guished feature is the presence of a microstructure
 210 transition for all the residence times. For a given
 211 residence time, a MT layer is formed as the first
 212 zone around fibers and then a sudden transition
 213 of the microstructure to HT carbon occurs at a
 214 certain axial position of the fiber bundle. Figure
 215 4 shows polarized light micrographs taken at the
 216 positions indicated in Fig. 3 for samples prepared
 217 at a residence time of 0.025 s and one can recog-
 218 nize a clear texture transition at the position (d).

219 Figure 5 compares the influence of various pre-
 220 cursors on the textures of pyrolytic carbon. In
 221 case of methane, a pressure of 10 kPa was applied,
 222 while a total pressure of 10 kPa and a partial pres-
 223 sure of 5 kPa are employed in case of ethanol to

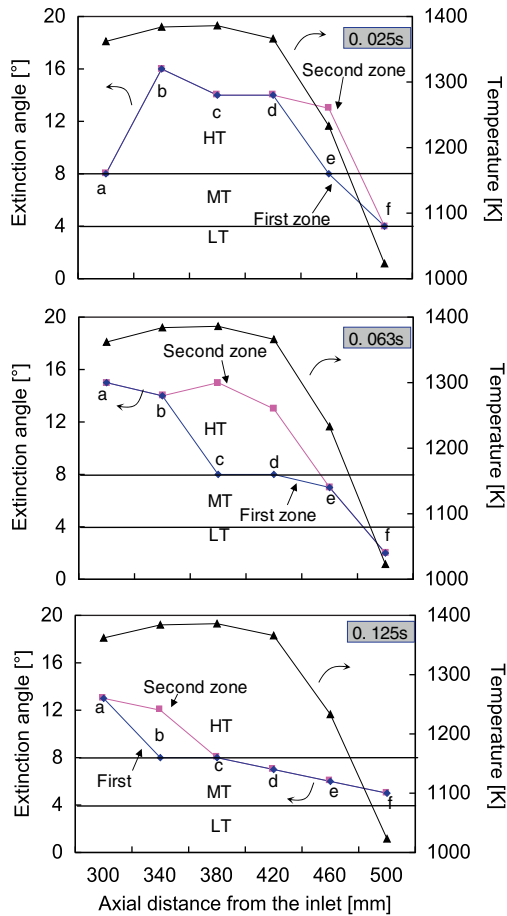


Fig. 3. Influence of the residence time on the extinction angle of pyrolytic carbon synthesized at $p(\text{C}_2\text{H}_5\text{OH}) = 5 \text{ kPa}$ and total pressure = 10 kPa.

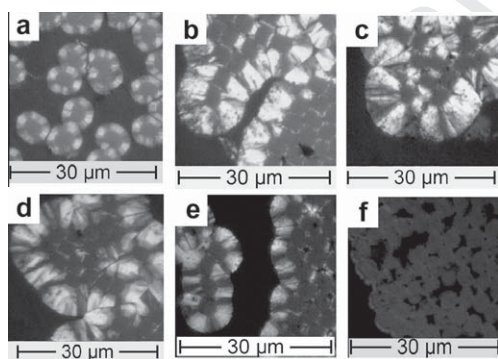


Fig. 4. Polarized light micrographs of pyrolytic carbon synthesized at $\tau = 0.025 \text{ s}$, $p(\text{C}_2\text{H}_5\text{OH}) = 5 \text{ kPa}$, total pressure = 10 kPa, $t = 10 \text{ h}$; (a-f) corresponds to the axial positions indicated in Fig. 3.

224
225

maintain the same initial concentration of carbon atoms in the gas-phase. Generally, a similar tex-

ture evolution of pyrolytic carbon is observed from the measured extinction angle profiles for both precursors. Methane, however, exhibits texture transition earlier than ethanol.

226
227
228
229

3.2. Carbon deposition rate

230

The influence of the residence time on the carbon deposition rate is shown in Fig. 6(a). A shorter residence time of 0.025 s leads to a maximum deposition rate at the position of the highest temperature, suggesting that ethanol or its direct decomposition products may form carbon. On the other hand, a longer residence time results in an earlier and faster deposition on the front part of the fiber bundle. Figure 6(b) compares the influence of various precursors on the deposition rate of pyrolytic carbon. It is obvious that ethanol exhibits a much higher deposition rate than methane even if the initial concentration of carbon atoms in the gas-phase is identical.

231
232
233
234
235
236
237
238
239
240
241
242
243
244

4. Kinetics and discussion

245

4.1. Gas-phase chemistry

246

To explore the effect of gas-phase chemistry on the formation of pyrolytic carbon from ethanol, the conversion in the gas-phase of the reactor are numerically simulated using a detailed reaction mechanism for the description of pyrolysis

247
248
249
250
251

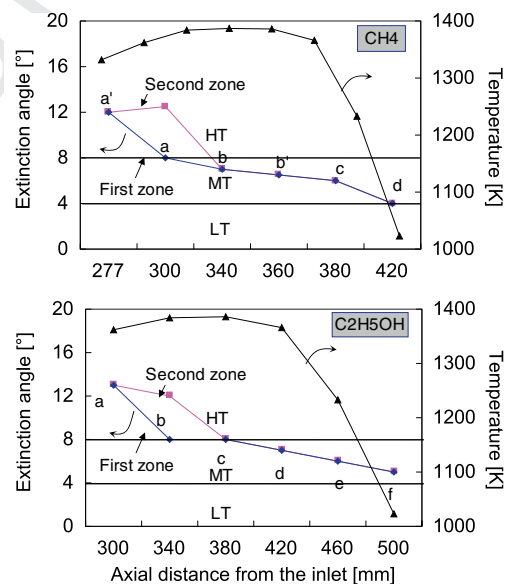


Fig. 5. Influence of precursors on the microstructure of pyrolytic carbon synthesized at $\tau = 0.125 \text{ s}$; $p(\text{C}_2\text{H}_5\text{OH}) = 5 \text{ kPa}$, total pressure = 10 kPa, densification time = 10 h (lower part) and 10 kPa CH_4 , densification time = 30 h (upper part).

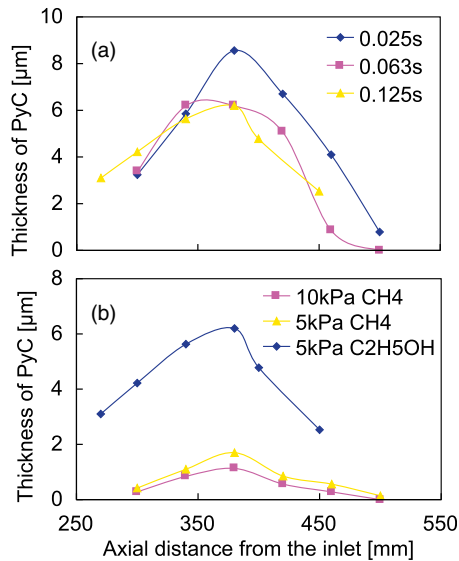


Fig. 6. Influence of processing parameters on the deposition rate of pyrolytic carbon synthesized at: (a) $p(\text{C}_2\text{H}_5\text{OH}) = 5 \text{ kPa}$, total pressure = 10 kPa, densification time = 10 h and various residence times; (b) various precursors with a residence time of 0.125 s, 10 h densification for ethanol and 30 h deposition time for methane, respectively.

of ethanol at temperatures near 1273 K. Involving 261 species and 1177 reversible reactions, the gas-phase reaction mechanism includes oxidation kinetics for hydrocarbons up to naphthalene and decomposition of hydrocarbons up to coronene [16,17]. Additionally, it includes the molecular weight growth reactions for PAH formation via the hydrogen-abstraction-acetylene-addition mechanism [18].

The proposed reaction mechanism of ethanol pyrolysis was applied to model experimental data published by Peg et al. [19]. In their experimental setup, a flow reactor made of quartz with an inner diameter of 45 mm and a length of 800 mm was employed allowing temperature (T) variations from 973 to 1473 K. Ethanol with a constant concentration of 50,000 ppm was fed into the reactor by saturating a nitrogen stream in an ethanol solution allowing a total flow rate of 1000 ml min^{-1} (STP). The gas residence time was determined as a function of the reaction temperature as: $\tau = 1706/T$. A non-dispersive one-dimensional plug flow model was used to simulate the experiments, and the corresponding gas velocity on the inlet is determined as: $V_{inlet} = 0.06T/1706$. Based on the detailed reaction mechanism, the DETCHEM^{PLUG} code [20] was employed to predict the gas-phase composition of this isothermal chemical reactor. Figure 7 shows the comparison of experimental results with the prediction of the plug model. Generally, molar fractions of CO, H₂, and

CO₂ increase with increasing temperature, while C₂H₂ and CH₄ concentrations are almost constant at higher temperatures. An acceptable agreement was achieved between the experimental data and the predicted results except for an over-prediction of acetylene and an under-prediction of ethane at higher temperatures. The deviation may result from both the imperfection of the reaction mechanism and an over-simplification of the reactor model. After evaluation of the reaction model, we are confident to use the mechanism in simulations of the species profiles of the reactor used in the current study.

4.2. Equilibrium calculations and kinetics

First, equilibrium calculations are conducted, in which the formation of solid carbon (graphite) is permitted using the DETCHEM^{EQUIL} code [20]; the simulation also includes all species of the detailed reaction mechanism proposed in the present work. For comparison, a reduced system is considered involving light hydrocarbons and CO, CO₂, and H₂O. Both results are illustrated in Fig. 8 (a) and (b). At temperatures around 1400 K the presence of solid carbon results in an equilibrium gas-phase consisting of only CO and H₂, while methane is the only stable hydrocarbon at temperatures below 800 K.

Pyrolysis of ethanol was modeled using a two-dimensional flow model coupled with the detailed reaction mechanism and numerical simulations corresponding to a run of an ethanol partial pressure of 5 kPa at a total pressure of 10 kPa, which were performed using the DETCHEM^{CHANNEL} code. The temperature profile shown in Fig. 1 is employed as the boundary condition. Figure 8(c) and (d) illustrate the influence of residence time on the axial distribution of dominant species in the gas-phase. A small residence time is helpful

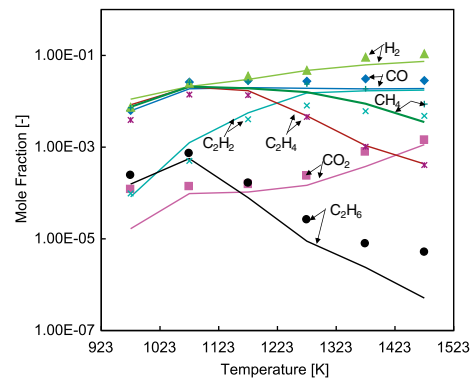


Fig. 7. Comparison of the gas-phase compositions predicted using the plug model (solid lines) with experimental results [19] (symbols) as a function of the operating temperature.

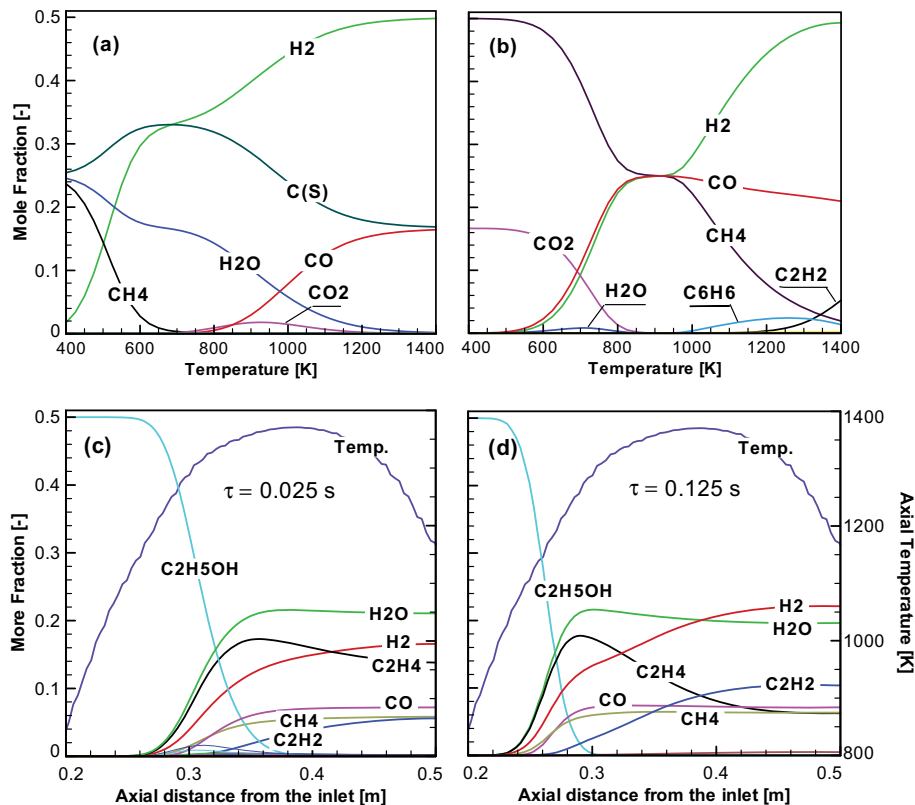


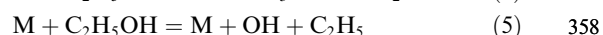
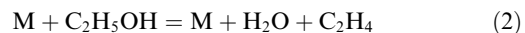
Fig. 8. Dominant species predicted by equilibrium calculations for isothermal, isobaric conditions with an initial C_2H_5OH partial pressure of 5 KPa and 10 kPa total pressure: (a) solid carbon and all gas-phase species involved in the reaction mechanism are considered, (b) only ethanol, CO, CO_2 , CH_4 , C_2H_4 , C_2H_2 , H_2 , H_2O , and C_6H_6 are considered; (c) dominant species distribution predicted by kinetic calculations with a residence time of 0.025 s, (d) with a residence time of 0.125 s.

321 to avoid pre-decomposition of ethanol before
 322 entering the isothermal part of the reactor under
 323 the present operating temperatures. The distinct
 324 evolution of the H_2/C_xH_y ratio from the inlet to
 325 the outlet corresponds to the significant decompo-
 326 sition of ethanol under a longer residence time. In
 327 spite of different residence times, the same domi-
 328 nant species, however, are present in the gas-phase
 329 including H_2 , H_2O , C_2H_4 , C_2H_2 , CO, and CH_4 . A
 330 shorter residence time leads to a smaller H_2/C_xH_y
 331 ratio, and may consequently, according to the
 332 hydrogen inhibition model of carbon deposition
 333 [12], lead to a bigger deposition rate as shown in
 334 Fig. 6(a). Compared with Fig. 8(a) and (b), it is
 335 obvious that the gas-phase composition shown
 336 in Fig. 8(c) and (d) is far away from equilibrium.

337 4.3. Reaction rate analysis

338 Reaction rate analysis of the pyrolysis of ethan-
 339 ol was conducted using a batch reactor model
 340 operated under conditions differing very much
 341 from those used in works published previously

[1–4]: a higher temperature (1373 K), shorter resi-
 342 dence time (0.001–0.125 s) and a lower ethanol
 343 partial pressure of 5 kPa at a total pressure of
 344 10 kPa. The DETCHEM^{BATCH} code was
 345 employed to numerically simulate homogeneous
 346 conversion in the gas-phase at isothermal and
 347 isobaric condition. Figure 9 illustrates the reac-
 348 tion rate analysis corresponding to a residence time
 349 of 0.025 s. All reaction channels contributing less
 350 than 5% to the total reaction flow are eliminated.
 351 Two reaction pathways in ethanol pyrolysis can
 352 be detected: One flow leads to the increase of the
 353 molecular weight of hydrocarbons and the other
 354 to the emission of CO and CO_2 . Among the four
 355 dissociation channels of ethanol,
 356



359 the first two reactions are dominant under the cur-
 360 rent CVD conditions, especially the first reaction

- 443 [3] G. Gupta, A. Deana, K. Ahn, R. Gorte, *Journal of*
444 *Power Sources* 158 (2006) 497–503. 469
- 445 [4] J. Li, A. Kazakov, F.L. Dryer, *International Journal*
446 *of Chemical Kinetics* 133 (2001) 859–867. 470
- 447 [5] E. Fitzer, L. Manocha, *Carbon Reinforcements and*
448 *Carbon/Carbon Composites*, Springer, Heidelberg,
449 Berlin, 1998. 471
- 450 [6] G. Savage, *Carbon–Carbon Composites*, Chapman
451 & Hall, London, 1992. 472
- 452 [7] A. Oberlin, *Carbon* 40 (1) (2002) 7–24. 473
- 453 [8] G. Vignoles, F. Langlais, C. Descamps, et al., *Surface*
454 *& Coatings Technology* 188–189 (2004) 241–249. 474
- 455 [9] Z.J. Hu, K.J. Hüttinger, *Carbon* 41 (8) (2003) 1501–
456 1508. 475
- 457 [10] K. Norinaga, Z.J. Hu, K.J. Hüttinger, *Carbon* 41
458 (8) (2003) 1509–1514. 476
- 459 [11] K. Norinaga, V.M. Janardhanan, O. Deutschmann,
460 *International Journal of Chemical Kinetics* 40 (2008)
461 199–208. 477
- 462 [12] A. Li, O. Deutschmann, *Chemical Engineering*
463 *Science* 62 (2007) 4976–4982. 478
- 464 [13] A. Li, K. Norinaga, W. Zhang, O. Deutschmann,
465 *Composites Science and Technology* 68 (2008) 1097–
466 1104. 479
- 467 [14] B. Reznik, K. Hüttinger, *Carbon* 40 (4) (2002) 621–
468 624. 480
- [15] B. Reznik, D. Gerthsen, E. Bortchagovsky, *Micros-*
copy 224 (2006) 322–327. 481
- [16] J.L. Emdee, K. Brezinsky, I. Glassman, *Journal of*
Physical Chemistry 96 (1992) 2151–2161. 482
- [17] K. Norinaga, O. Deutschmann, *Industrial & Engi-*
neering Chemistry Research 46 (2007) 3547–3557. 483
- [18] M. Frenklach, J. Warnatz, *Combustion Science and*
Technology 51 (1987) 265–283. 484
- [19] Peg, M., Ruiz, M.P., Millera, A., Bilbao, R.,
Alzueta, M.U., Proceedings of the European Com-
bustion Meeting, The Combustion Institute, Cha-
nia, Greece, 2007. 485
- [20] O. Deutschmann, S. Tischer, S. Kleditzsch, et al., H.
Minh, DETCHEM Software Package, 2.1 ed.,
www.detchem.com, Karlsruhe, 2007. 486
- [21] M. Lieberman, H. Pierson, *Carbon* 12 (1974) 233–
241. 487
- [22] H. Pierson, M. Lieberman, *Carbon* 13 (1) (1975)
159–166. 488
- [23] W. Zhang, Z. Hu, K. Hüttinger, *Carbon* 40 (14)
(2002) 2529–2545. 489
- [24] W. Zhang, K. Hüttinger, *Carbon* 41 (12) (2003)
2325–2337. 490
- [25] B. Ruf, F. Behrendt, O. Deutschmann, J. Warnatz,
Surface Science 352–354 (1996) 602–606. 491
- 492
493
494